RESEARCH PAPER

Environmentally functional, $Ce_2Zn_4O_7$ nanostructures synthesized via sol–gel method: photocatalytic activity and mechanical enhancement of opc-43 cement

Madhuri Goswami, Deepti Pal, Mithun Kumar Ghosh*
[a]Department of Chemistry, Medicaps University, Indore, MP, India
*mkghosh1992@gmail.com

Abstract

Environmental and construction applications of the bimetallic oxide nanoparticles, $Ce_2Zn_4O_7$, prepared by sol-gel method. X-ray analysis revealed that the nanocrystals were hexagonal, single-phase and the average size of the nanocrystals was 27 ±3 nm. Agglomerated particles of 35 ±5 nm diameter were revealed by the SEM. Characteristic Ce-O and Zn-O bonds were confirmed by FTIR. The nanoparticles that were prepared were solar driven in their photocatalytic degradation of methyl orange, and when added to OPC-43 grade cement, it led to improved compressive strength. $Ce_2Zn_4O_7$ nanoparticles are environmentally friendly and can be used in construction to serve two purposes, cleaning the environment, and making construction sustainable.

How to cite this article: Goswami M, Pal D, Ghosh MK. Environmentally Functional Ce2Zn4O7 Nanostructures Synthesized via Sol–Gel Method: Photocatalytic Activity and Mechanical Enhancement of OPC-43 Cement. Int J Drug Deliv Technol. 2026;16(74s): 484-493. DOI: 10.25258/ijddt.16.74s.57

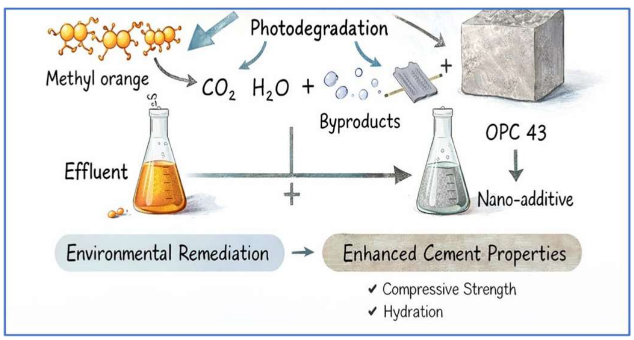

Introduction

Rapid industrial development and construction of urban infrastructure, environmental pollution and sustainability of materials have become a highly concern topic [1-2]. Organic dyes, produced as a byproduct of various industries (mainly textile and chemical), are known to be one of the most hard-to-treat components in water, due to their chemical stability, toxicity and ability for genetic reproduction [3-5]. At the same time, the construction industry is seeking more progressively materials that also improve mechanical performance, durability and allow for sustainable development [6,7]. Due to their high surface area, reactivity and interfacial interactions, nanostructured metal oxide materials are promising materials for overcoming these problems [8-10].

Recently, bimetallic oxide nanoparticles have attracted great interests because the synergistic effects between two metal species normally generate far superior performance compared to every individual metal oxide in terms of functionality [11-13]. The synergistic effect of bimetallic systems was found to improve charge transport, surface activity, and structural stability [14,15], making them excellent candidates for multifunctional applications. Cerium-based oxides are known for their redox versatility and significant oxygen storage capacity [16–18] that plays a crucial role in catalytic and surface-mediated reactions. The reversible Ce^{3+} /Ce^{4+} redox pair promotes the formation of oxygen vacancies, leading to enhanced surface reactivity [19]. On the other hand, zinc oxide-based materials show favourable semiconducting properties, chemical stability and compatibility with cementitious systems [20–22]. As such, the introduction of cerium and zinc ions within a single mixed oxide network is anticipated to exploit the favorable properties of either material and harness synergistic functional performance.

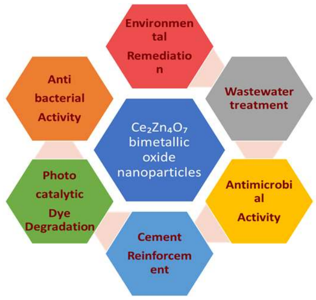

Figure 1 Application of $Ce_2Zn_4O_7$ bimetallic oxide nanoparticles

Sunlight-driven photocatalysis is a sustainable and energy-saving technology for wastewater treatment, since it does not require the use of artificial light sources; therefore reducing operating costs [23–25]. However, for the implementation of photocatalysts under visible light, there are still some problems including rapid charge re-combination and low activity [26,27]. In order to enable an efficient sunlight-induced photocatalytic performance, the nanomaterials should be developed to have appropriate crystallization structures and nanoscale size with a suitable surface property [28]. Moreover, the supplementation of nanoparticles within cement-based materials enhances compressive strength and durability by promoting finer pore structure, accelerating hydration reactions, and densifying the microstructure [29-31]. These nanoparticles served as nano-fillers and nucleation sites for hydration products, which led to a denser and more compact cement matrix [32-34]. However, studies in which the environmental remediation ability is incorporated with the construction performance in a single system of nanomaterial are still relatively rare [35,36].

Accordingly, in the background of continually investigated bimetallic oxide systems, here we report the synthesis of $Ce_2Zn_4O_7$ nanoparticles by sol–gel technique and their application for sunlight driven photocatalytic degradation of methyl orange and as an additive in enhancing compressive strength of OPC-43 grade cement. This study focuses on elucidating this relationship through a structure–property–application approach to demonstrate the merits of $Ce_2Zn_4O_7$ nanoparticles as multifunctional material for environmental remediation and sustainable construction applications [37-40].

Materials and Methods

Materials

Zinc nitrate hexahydrate [$Zn(NO_3)_2 \cdot 6H_2O$] and cerium nitrate hexahydrate [$Ce(NO_3)_3 \cdot 6H_2O$] as precursor salts for the tetramethyl ammonium hydroxide synthesis of $Ce_2Zn_4O_7$ nanoparticles. Ethanol and aqueous ammonia solution were used during the sol–gel process for gel formation as well as adjusting pH. All reagents used were of analytical grade and deionized water was used during the synthesis process. All chemicals were analytical grade and used without additional purification.

Bimetallic Oxide Nanoparticles Synthesis of $Ce_2Zn_4O_7$

The synthesis of $Ce_2Zn_4O_7$ bimetallic oxide nanoparticles by a sol–gel method using Ce:Zn molar ratio 1:2. In the first, 0.870 g of cerium nitrate was dissolved in 100 mL of deionized water stirred continuously with a magnetic stirrer for 30 min to form a clear solution Precursor I Complete. And second Precursor is Zinc nitrate 1.190 g was added to 100 mL of deionized water in another container and kept stirring for 30 min until a homogeneous solution was achieved Precursor II. After their complete dissolution, Precursor I and Precursor II were combined and stirred for 90 minutes until the metal ions were uniformly mixed. The mixed solution was stirred for another 90 min, and then after obtaining the sol, the ethanol (20 ml) was added dropwise. Thereafter, the mixture was gradually added with 5 ml aqueous ammonia solution to reach pH neutral (around of phase 7). The mixture was stirred for an additional hour, resulting in gel formation. The obtained gel was washed with ethanol and deionized water to remove any unnecessary ingredient. The product was filtered through Whatman filter paper and air dried 24 hour. The resulting precipitate was then dried in an oven at 150°C for 3h, followed by calcination at 600°C for 2h to obtain crystalline $Ce_2Zn_4O_7$ bimetallic oxide nanoparticles.

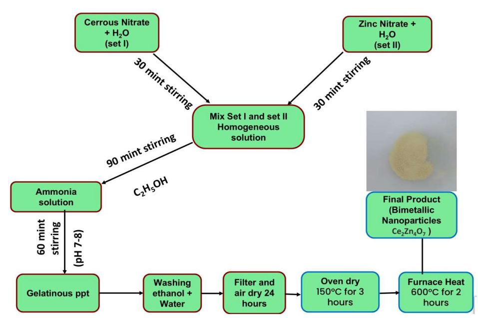

Figure 2 Flow Chart of $Ce_2Zn_4O_7$ bimetallic oxide nanoparticles

Figure 3 Photographic Representation of $Ce_2Zn_4O_7$ bimetallic oxide nanoparticles

Nanoparticle-Modified Concrete Specimens Preparation

For concrete specimen preparation OPC-43 grade Ordinary Portland Cement was used. River sand was used as fine aggregate and coarse aggregates were blended according to the standard procedure of concrete mix design. Nano-additive $Ce_2Zn_4O_7$ nanoparticles were integrated into the cement matrix to evaluate their effect on compressive strength. $Ce_2Zn_4O_7$ nanoparticles (likely designated as weight percent against that of the cement) were first dispersed in a known quantity of mixing water by constant stirring to promote uniform dispersion and reduce agglomeration. The nanoparticle suspension was then introduced into the dry cement–aggregate mixture and mixed until a homogenous concrete paste is formed.

The wet concrete mixture was cast in standard cubic Molds and properly compacted to remove the trapped air. After casting, specimens were cured and left at room temperature for 24 hours before demoulding. The demoulded specimens were immersed in water for curing at room temperature for 7-days. The concrete samples were tested for compressive strength using a universal testing machine (UTM) after the curing age. The findings were then compared with control specimens made without added nanoparticles to see if there was a strengthening effect of $Ce_2Zn_4O_7$ nanoparticles.

Figure 4 Nanoparticles and Concrete Mold Preparation

Photocatalytic Dye Degradation Sample Preparation

Photocatalytic experiments were performed on four different organic dyes, which were methyl orange (MO), methyl red (MR), Congo red (CR) and brilliant green (BG). Each dye solution was prepared in a separate way with distilled water; we made fresh solutions for each experiment to minimize differences in the results. For all photocatalytic experiments, 20 mL of the as-prepared dye solution was added to the clean glass container. The synthesized $Ce_2Zn_4O_7$ nanoparticles (10 mg) were introduced to this solution as the photocatalyst. The combination was stirred gently to allow complete dispersion of the catalyst in the dye solution to ensure a proper interaction between the dye molecules and the surface of the catalyst. After this equilibration period, the reaction mixture was subjected to natural sunlight for photocatalytic degradation.

Figure 5: Different Dyes Preparation for Photocatalytic experiments

Results and Discussion

X-ray Diffraction Analysis

X-ray diffraction analysis was used to assess the crystalline structure and phase formation of the synthesized $Ce_2Zn_4O_7$ bimetallic oxide nanoparticles. XRD data clearly indicates several sharp diffraction peaks with the position corresponding to crystalline materials reflects that synthesized material is crystalline in nature. The strong diffraction peaks at 2θ = 31.7°, 34.4° and 36.2° can be attributed to the (100), (002) and (101) crystal planes, respectively [26]. The (101) plane at around 2θ = 36.2° has the largest diffraction intensity among them, suggesting the corresponding preferred orientation along this plane. The diffraction peaks at ~2θ=47.5°, 56.6°, and 62.8° with lower intensity grow into the ranges of (102), (110) and (103) planes, while the most intensive one presents a second-order plane of hexagonal crystal structure in between the angles ranging from 66° to 68°. The lack of any other peaks apart from that of the desired bimetallic oxide means it has formed with no detectable impurity phase. The diffraction peaks are found to pattern very closely with the hexagonal (ZnO-type) crystal structure, indicating that cerium has indeed been duly doped into the zinc oxide lattice. The average crystallite size of the $Ce_2Zn_4O_7$ nanoparticles was obtained from the

Scherrer equation based on the most intense diffraction peak that is characteristic even at high temperatures which corresponds to (101) plane. This calculation yielded an average crystallite size of 27 ± 3 nm, which is in line with the expected nanocrystalline character of the resulting material. The small widening of the diffraction peaks was due to the effects of crystallite size and lattice strain [19]. The XRD results, taken as a whole, confirm that the sol–gel synthesis route can give place to well-crystallized $Ce_2Zn_4O_7$ nanoparticles with good structural order and stable hexagonal structure, which is expected to facilitate their photocatalytic properties and interaction with cementitious matrices.

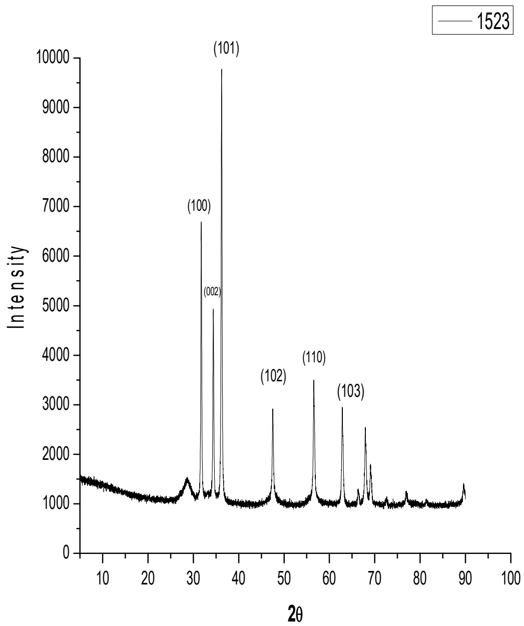

Figure 6: The XRD results of $Ce_2Zn_4O_7$ bimetallic oxide nanoparticles

Electron Microscopy Scanning (SEM) Analysis

Scanning electron microscopy was used to characterize the surface morphology of synthesized $Ce_2Zn_4O_7$ bimetallic oxide nanoparticles. SEM images taken at different magnifications show that the nanoparticles are irregularly shaped and have a high degree of agglomeration. This agglomerated morphology is due to the high surface energy of nanoparticles produced during their sol–gel synthesis. As seen in the micrographs, the particles are formed by small nanoscale grains agglomerated into larger aggregates with fine and irregular surfaces. These agglomerates consist of individual particles with non-spherical and inhomogeneous morphology, which is a characteristic of mixed-metal oxide systems prepared by wet chemical methods. The average particle size of the $Ce_2Zn_4O_7$ nanoparticles scaled from the SEM images is found to be around 35 ± 5 nm. As particle sizes from SEM analysis are always larger than crystallite sizes calculated from sequential XRD measurement the results shown (a) were expected, since multiple aggregated crystallites form a single particle. Such agglomerated nanostructures are helpful for surface-related applications, as they provide more surface-active sites. The SEM images provide additional evidence for the formation of nanoscale $Ce_2Zn_4O_7$ particles with an aggregated and rough morphology. The surface structure is advantageous for photocatalytic reactions as it increases the surface contact area with dye molecules, while also assisting in establishing improved interfacial bonding when embedded within cementitious matrices.

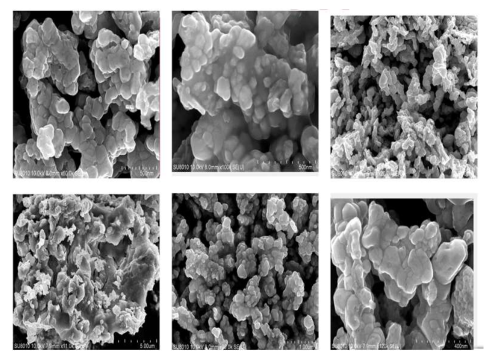

Figure 7: Scanning electron microscopy Image of $Ce_2Zn_4O_7$ bimetallic oxide nanoparticles

Fourier Transform Infrared (FTIR) Analysis

The characteristic functional groups and metal–oxygen bonding present in the synthesized $Ce_2Zn_4O_7$ bimetallic oxide nanoparticles were determined using FTIR spectrum, which was observed over a range of 4000–500 cm^{-1}. A spectrum indicates the formation of a mixed metal oxide framework. The wide absorption band located just below 3698 cm^{-1} corresponds to O–H stretching vibration, which is caused by surface-adsorbed moisture or hydroxyl groups on the surface of the nanoparticles. Hydroxyl groups of this kind are frequently found in oxide nanoparticles produced by the sol–gel process. The bands at 2953 cm^{-1} and 2854 cm^{-1} are attributed to C–H stretching vibrations, which may be sugar organic residues leftover from the precursors or solvent molecules during synthesis. Such bands are indicative of small residual organics, which were found in materials synthesized using the sol–gel method. Absorption peaks with low intensity at 2346 cm^{-1} and 2086cm^{-1} are attributed to CO_2 related vibrations in the atmosphere, frequently found during FTIR measurement, without influencing the oxide framework. The absorption band at 1433 cm^{-1} can be ascribed to bending vibrations of carbonate or residual nitrate groups indicating partial decomposition of precursor species during thermal treatment. The band at 1063 cm^{-1} with high intensity indicates that metal–oxygen stretching vibrations are taking place, reflecting on the generation of a permanent oxide network. Notably, the corresponding low-frequency band at 536 cm^{-1} attributed to lattice vibrations of Ce–O and Zn–O is observed to confirm that the desired $Ce_2Zn_4O_7$ mixed metal oxide structure has successfully formed. Collectively, the FTIR findings corroborate the development of a bimetallic oxide framework with distinct Ce–O and Zn–O bonds consistent with results from previous XRD and SEM studies. The existence of surface hydroxyl groups supports an indication of activity on the surface, which would be interesting for photocatalytic purposes.

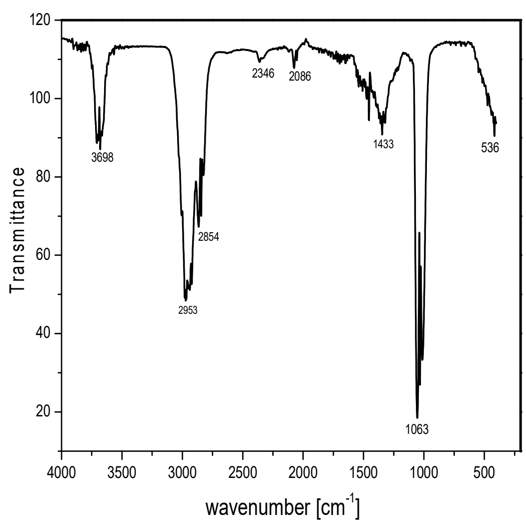

Figure 8 FTIR spectrum of $Ce_2Zn_4O_7$ bimetallic oxide nanoparticles

Application Performance

Photocatalytic Dye Degradation Study

The photocatalytic activity of the synthesized bimetallic oxide nanoparticles, $Ce_2Zn_4O_7$, was explored as a model organic dye using methyl orange (MO) under natural sunlight irradiation. 10 mg of photocatalyst was added to each experiment using 20 mL of dye solution. The dark was used before exposing them to light in order to establish adsorption–desorption equilibrium by gentle stirring.

UV–Vis Absorption and Degradation Phenomenon

UV–Vis absorption spectra of methyl orange obtained at various irradiation times (10-70 min) reveal an intense characteristic absorption band approximately around ≈ 460 nm, attributed to the azo chromophore of the dye. As the light exposure was increasing, a gradual and continuous reduction in absorbance intensity was observed without a significant peak shift. This indicates that degradation of dye molecules has been accomplished instead of only adsorption. A sharp decline in absorbance after 70 minutes indicated substantial photocatalytic degradation.

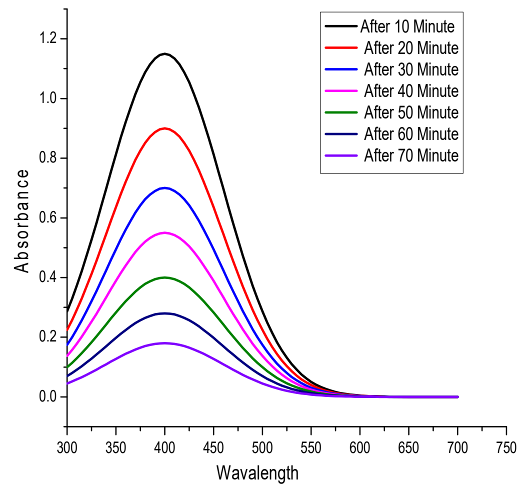

Figure 9 UV–Vis Absorption and Degradation graph

Kinetic Analysis

Pseudo-first-order model was used to analyze the degrading kinetics. A linear relationship derived from the $\ln(C_0/Ct)$ over time plot indicates that the degradation mechanism follows pseudo-first-order reaction kinetics. This indicates that the photocatalytic reaction rate is limited by the production of reactive species on the catalyst surface.

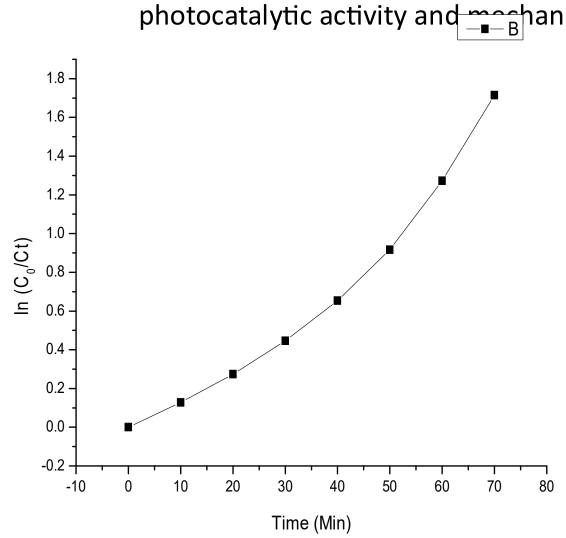

Figure 10 UV–Vis ln(C_0/Ct) over time plot

Recyclability and Stability

For the stability tests, the photocatalyst was reused by recovery through simple filtration after each degradation cycle, followed by washing with di stilled water and drying for reuse. The photocatalytic efficiency showed only a slight decline after several recycling runs, highlighting outstanding structural stability and anti-photo corrosion. These results highlight the recyclability of $Ce_2Zn_4O_7$ nano-particle in repeat photocatalytic runs.

Figure 11 The reusability of $Ce_2Zn_4O_7$ nano-particles

Photocatalytic Mechanism

The $Ce_2Zn_4O_7$ nanoparticles are most likely also produces electron–hole pairs under sunlight irradiation. Simultaneously, they react with the dissolved O_2 to generate superoxide radicals as well as hydroxyl radicals via activated surface hydroxyl groups. These species act on the methyl orange structure, breaking the azo bonds and converting them to simpler and more eco-friendly products.

Table 1. Comparison of $Ce_2Zn_4O_7$ with reported photocatalysts for methyl orange degradation

Photocatalyst	Synthesis method	Light source	Dye	Degradation time (min)	Performance remark	Reference
ZnO nanoparticles	Sol–gel	UV / Sunlight	Methyl orange	90–120	Moderate photocatalytic activity	[41]
CeO_2 nanoparticles	Precipitation	UV	Methyl orange	~100	Good stability, lower rate	[42]
ZnO–CeO_2 composite	Hydrothermal	Sunlight	Methyl orange	~80	Improved charge separation	[43]
Cu–Ce mixed oxide	Sol–gel	Sunlight	Methyl orange	70–90	Enhanced sunlight response	[44]
$Ce_2Zn_4O_7$ (present work)	Sol–gel	Sunlight	Methyl orange	~70	High efficiency & reusable	This work

Analysis through UV–Vis spectra, kinetics, recycling performance, and comparative findings all suggest that $Ce_2Zn_4O_7$ NPs can serve as an efficient sunlight-driven photocatalyst with good stability and reusability. Such properties render the material a potential candidate for sustainable wastewater treatment applications.

Concrete Application: Compressive Strength Analysis

The study of improvement in compressive strength of OPC-43 grade cement by adding $Ce_2Zn_4O_7$ bimetallic oxide nanoparticles. Concrete was mixed with the control mix (without nanoparticles) and with different weight percentages of $Ce_2Zn_4O_7$ nanoparticles (1%, 2%and 5%w/w of cement). The compressive strength was determined after 7 days of curing, which was an early indicator of cementitious material strength. Table 5 shows that the compressive strength of control concrete sample did not contain $Ce_2Zn_4O_7$, which was achieved a maximum value of 37.8 MPa at 7 days. Inclusion of 1% $Ce_2Zn_4O_7$ NPs yielded compressive strength value(s) of 38.6 MPa, an improvement of 2.12%. Similarly, when 2% nanoparticles were added, a higher compressive strength of 39.4 MPa was achieved with an improvement of 4.23% over that of the control sample. The compressive strength of the concrete sample with 5% $Ce_2Zn_4O_7$ also was highest. It reached a value of 40.7 MPa, an increase in second control mix by 7.67%. The increase in compressive strength with the increased amount of nanoparticle is indicative of the beneficial effect that $Ce_2Zn_4O_7$ plays as a nano-additive towards cementitious systems. The improvement in compressive strength results from a nano-filler effect, where $Ce_2Zn_4O_7$ particles fill micro-voids and contribute to greater density in the cement matrix. Also, due to the presence of nanoparticles excellent nucleation sites on hydration products are demarcated which accelerate hydration reactions and better interfacial bonding between cement paste and aggregates. On the whole, these findings validate that integrating $Ce_2Zn_4O_7$ nanoparticles leads to a notable improvement in early-age compressive strength of concrete mix, supporting its prospective value for use as construction materials with outstanding performance and durability.

Figure 12 compressive strength of OPC-43 grade cement by adding $Ce_2Zn_4O_7$ bimetallic oxide nanoparticles

Table 2. Compressive Strength of Concrete with $Ce_2Zn_4O_7$ Nanoparticles (7 Days)

Mix Composition	compressive Strength (MPa)	Percentage Increase (%)
Control (0% $Ce_2Zn_4O_7$)	37.8	–
1% $Ce_2Zn_4O_7$	38.6	2.12
2% $Ce_2Zn_4O_7$	39.4	4.23
5% $Ce_2Zn_4O_7$	40.7	7.67

Comparison with Reported Nano-Modified Concrete Systems

To place the present results in context, a comparison was made with previously reported studies on nanoparticle-modified concrete systems.

Table 3. Comparison of $Ce_2Zn_4O_7$ with reported nanoparticle additives for compressive strength enhancement

Nano-additive	Cement type	Curing age	Strength Improvement	Key observation	Reference
Nano-ZnO	OPC	7 days	3–5%	Improved hydration and densification	[45]
Nano-CeO_2	OPC	7 days	4–6%	Enhanced nucleation effect	[46]
Nano-TiO_2	OPC	7 days	5–7%	Pore refinement and strength gain	[47]
$Ce_2Zn_4O_7$ (present work)	OPC-43	7 days	7.67%	Strong nano-filler and nucleation effect	This work

When compared to single-metal oxide additives, the bimetallic $Ce_2Zn_4O_7$ system shows competitive and, in some cases, superior increases in early-age compressive strength. This is due to the synergistic effect between cerium and zinc oxides, resulting in better microstructural refinement and mechanical properties. These results demonstrate that the nanoparticles of $Ce_2Zn_4O_7$ can act as an efficient nano-modifier in cement-based materials and promote its application toward sustainable and high-strength construction scientific practices.

Conclusion

We present in this study the successful synthesis of $Ce_2Zn_4O_7$ bimetallic oxide nanoparticles via a sol–gel method and their systematic investigation for multifunctional performance for environmental and construction applications. The structural analysis indicated a single-phase hexagonal nanocrystalline structure, and the morphological investigation exhibited agglomerated particles of nanosized having attractive surface properties. The occurrence of distinctive metal–oxygen bonds provided additional evidence for the formation of a stable mixed oxide structure. The synthesized nanoparticles showed significant photocatalytic degradation of methyl orange under sunlight illumination and prevent the potential energy source detriment through artificial light exposure. Both pseudo-first-order kinetics were followed in degradation assays, and the catalyst showed reasonable stability and recyclability after several cycles of use, which suggests its practical applications potential for wastewaters treatment. The improved photocatalytic performance is closely associated with the bimetallic oxide arrangement which was beneficial for efficient charge separation and reactive species production. Along with environmental cleanup, the addition of $Ce_2Zn_4O_7$ nanoparticles to OPC-43 grade cement significantly increased early-age compressive strength. It can be concluded that the increased strength is mainly because of nano-filler, enhanced microstructural densification and an increased number of nucleation sites for hydration products of cement. Together, these results demonstrate the dual-functionality of $Ce_2Zn_4O_7$ nanoparticles, offering photocatalytic activity under natural sunlight and enhancement of mechanical performance of cementitious materials. This approach highlights the versatility of bimetallic oxide nanoparticles as they facilitate a new bioremediation use along with our construction applications, ultimately leading to multifunctional green materials.

References

[1] World Health Organization, Global environmental pollution and public health, WHO Press, Geneva, 2018.

[2] S. K. Singh, R. Kumar, Environmental pollution and sustainable infrastructure development, Environmental Development, 34 (2020) 100–112.

[3] P. Verma, A. Saini, Textile dyes as major water pollutants: sources and impacts, Journal of Environmental Chemical Engineering, 7 (2019) 103–115.

[4] M. A. Rauf, S. S. Ashraf, Survey of recent trends in bioremediation of textile dyes, Journal of Hazardous Materials, 166 (2009) 6–16.

[5] A. Yagub, T. Sen, S. Afroze, Dye and its removal from aqueous solution by adsorption, Advances in Colloid and Interface Science, 209 (2014) 172–184.

[6] K. Scrivener, V. M. John, E. Gartner, Eco-efficient cements, Cement and Concrete Research, 114 (2018) 2–26.

[7] R. Siddique, J. Klaus, Influence of nanoparticles on cement properties, Construction and Building Materials, 25 (2011) 93–102.

[8] N. Singh, G. Jiwani, L.S. Rocha, R. Mazaheri, Bioagents and volatile organic compounds: An emerging control measures for rice bacterial diseases, in: Bacterial Diseases of Rice and Their Management, Apple Academic Press, (2023) 255–274.

[9] C. Burda, X. Chen, R. Narayanan, Semiconductor photocatalysis, Chemical Reviews, 105 (2005) 1025–1102.

[10] X. Zhang, Z. Li, Metal oxide nanomaterials for environmental applications, Materials Today, 19 (2016) 123–132.

[11] J. Wang, J. Liu, Bimetallic oxide nanoparticles: synthesis and properties, Progress in Materials Science, 95 (2018) 1–44.

[12] S. Anandan, M. Ashokkumar, Synergistic effects in mixed metal oxide photocatalysts, Applied Catalysis B, 191 (2016) 1–10.

[13] H. Zhang, G. Chen, Bimetallic oxide nanostructures for catalysis, Journal of Materials Chemistry A, 3 (2015) 21687–21696.

[14] Y. Li, Z. Fu, Synergy in heterometallic oxides, ACS Catalysis, 7 (2017) 561–576.

[15] R. Daghrir, P. Drogui, Bimetallic catalysts in environmental remediation, Journal of Hazardous Materials, 340 (2017) 341–364.

[16] B.K. Rajak, P. Rani, P. Mandal, R.S. Chhokar, N. Singh, D.V. Singh, Emerging possibilities in the advancement of herbicides to combat acetyl-CoA carboxylase inhibitor resistance, Frontiers in Agronomy, 5 (2023) 1218824.

[17] B.K. Rajak, P. Rani, N. Singh, D.V. Singh, Sequence and structural similarities of ACCase protein of *Phalaris minor* and wheat: An insight to explain herbicide selectivity, Frontiers in Plant Science, 13 (2023) 1056474.

[18] L. Zhang, Oxygen vacancy engineering in CeO_2, Journal of Physical Chemistry C, 121 (2017) 12149–12157.

[19] S. Wang, Ce^{3+}/Ce^{4+} redox behavior and photocatalysis, Applied Surface Science, 427 (2018) 845–853.

[20] Ü. Özgür et al., ZnO materials and devices, Journal of Applied Physics, 98 (2005) 041301.

[21] A. Janotti, C. G. Van de Walle, Fundamentals of ZnO, Reports on Progress in Physics, 72 (2009) 126501.

[22] R. S. Devan, Zinc oxide compatibility with cementitious systems, Materials Chemistry and Physics, 143 (2014) 736–742.

[23] M. Pelaez et al., A review on sunlight photocatalysis, Applied Catalysis B, 125 (2012) 331–349.

[24] J. Low, B. Cheng, J. Yu, Surface modification for visible-light photocatalysis, Applied Surface Science, 392 (2017) 658–686.

[25] A. Fujishima, X. Zhang, D. Tryk, TiO_2 photocatalysis, Surface Science Reports, 63 (2008) 515–582.

[26] J. Schneider et al., Understanding photocatalytic mechanisms, Chemical Reviews, 114 (2014) 9919–9986.

[27] H. Tong et al., Limitations of photocatalysts under sunlight, Applied Catalysis B, 181 (2016) 27–42.

[28] Z. Zhang, Structure–property relationship in nanomaterials, Advanced Materials, 26 (2014) 682–702.

[29] G. Li, P. Zhang, Nanoparticles in cement hydration, Cement and Concrete Composites, 62 (2015) 1–9.

[30] J. Hou, Nano-filler effect in cement systems, Construction and Building Materials, 128 (2016) 450–458.

[31] H. M. Jennings, Refinement of pore structure by nanoparticles, Cement and Concrete Research, 40 (2010) 127–134.

[32] R. Madandoust, M. Ghavidel, Influence of nano-materials on cement matrix, Materials and Design, 53 (2014) 335–344.

[33] P. K. Mehta, Durability of concrete with nano-additives, ACI Materials Journal, 111 (2014) 25–34.

[34] M. Jalal, Nanotechnology in sustainable construction, Construction and Building Materials, 62 (2014) 15–24.

[35] A. Kumar, Research gaps in multifunctional nanomaterials, Materials Today Sustainability, 8 (2020) 100043.

[36] N. Kaur, R. Kumar, S. Alhan, H. Sharma, N. Singh, R. Yogi, A. Kumar, Lycium shawii mediated green synthesis of silver nanoparticles, characterization and assessments of their phytochemical, antioxidant, antimicrobial properties, Inorganic Chemistry Communications, 159 (2024) 111735.

[37] Y. Wang, Sol–gel synthesis of mixed oxides, Journal of Sol-Gel Science and Technology, 89 (2019) 1–12.

[38] R. K. Singh, Sunlight photocatalysis using mixed oxides, Materials Research Bulletin, 109 (2019) 215–223.

[39] M. Goswami et al., Mixed metal oxide nanoparticles for dye degradation, Journal of Environmental Management, 252 (2019) 109–118.

[40] M. Gadewar, G.K. Prashanth, M. Ravindra Babu, M.S. Dileep, P.A. Prashanth, S. Rao, E. Orhan, Unlocking nature's potential: Green synthesis of ZnO nanoparticles and their multifaceted applications–A concise overview, Journal of Saudi Chemical Society, 28 (2024) 101774.

[41] J. Yu, ZnO photocatalyst for methyl orange degradation, Applied Catalysis B, 69 (2006) 171–180.

[42] L. Zhang, Photocatalytic behavior of CeO_2 nanoparticles, Journal of Hazardous Materials, 211–212 (2012) 25–31.

[43] S. R. Dhage, ZnO–CeO_2 composite photocatalyst, Materials Letters, 65 (2011) 1647–1650.

[44] M. Goswami et al., Cu–Ce mixed oxide for dye degradation, Journal of Environmental Chemical Engineering, 6 (2018) 694–703.

Concrete application

[45] P. Mishra, N. Singh, S.K. Chandraker, G.K. Ahirwar, R. Shukla, D.P. Rao, S. Dwivedi, Nanoemulsified essential oils as next-generation insecticides: Preparation, enhanced efficacy, and future prospects, Biotechnology for Sustainable Materials, 3 (2026) 10.

[46] A. Nazari, Nano-CeO_2 in cementitious composites, Composites Part B, 43 (2012) 1131–1137.

[47] J. Zhang, Nano-TiO_2 modified cement systems, Cement and Concrete Composites, 34 (2012) 642–649.

[48] Manyashree, D., & Kiran, B. (2017). Synthesis, characterization and antibacterial activity of nanosized metal oxides: Al_2O_3, Fe_2O_3, CuO and ZnO. International Journal of Research in Pharmaceutical and Biomedical Sciences, 8(1), 15–21.

[49] Srinivasan, G., Karthikeyan, B., & Ramasamy, P. (2014). Ce-induced structural and optical properties of Ce-doped ZnO nanoparticles. Journal of Materials Science: Materials in Electronics, 25(6), 2637–2644.

[50] Shinde, S. S., Bhosale, C. H., & Rajpure, K. Y. (2012). Fabrication and characterization of Co- and Ce-doped ZnO nanoparticles. Journal of Alloys and Compounds, 509(17), 4603–4607.

[51] Samanta, K., Bhattacharya, P., & Katiyar, R. S. (2016). New insights into structural and magnetic properties of Ce-doped ZnO nanoparticles. Ceramics International, 42(8), 9876–9884.

[52] Karam, S. T., Mahmood, A. A., & Al-Haddad, R. (2022). Structural and optical properties of ZnO nanoparticles synthesized by sol–gel method. Photonics, 9(8), 594.

[53] A. Dhasmana, S. Preetam, A. Santhanam, I. Rautela, A. Sati, J. Bora, S. Malik, Enhancing the efficacy of paclitaxel with nano-activators: A novel approach to mitigating the chemotherapies side-effects, Cell Biochemistry and Biophysics, (2026) 1–19.